SciEn
Journal of Engineering Advancements Vol. 06(03) 2025, pp 75-85 https://doi.org/10.38032/jea.2025.03.001

A Numerical Analysis of NACA 0015 Airfoil with Different Types of Flaps

Simanto Das, Md. Atikur Rahman Khan, Sudipto Kumar Dash, Eyasin Hossain Sayeed, Md. Mehdi Masud Talukder*

Department of Mechanical Engineering, Chittagong University of Engineering and Technology, Chattogram-4349, Bangladesh

Received: March 17, 2025, Revised: August 05, 2025, Accepted: August 09, 2025, Available Online: September 04, 2025

ABSTRACT

Enhancing aerodynamic performance is critical in the aviation industry to improve aircraft efficiency and reduce fuel consumption. Airfoils, which generate lift and drag during motion through a fluid, are highly sensitive to geometric modifications. This study investigates the aerodynamic behavior of a NACA 0015 airfoil equipped with various flap configurations and flap deflection angles. Flaps are widely used to increase the camber and effective angle of attack of an airfoil, thereby enhancing lift generation. The NACA 0015 airfoil was modeled using SOLIDWORKS, and computational fluid dynamics (CFD) simulations were performed in ANSYS Fluent, employing the k-ω SST turbulence model at a Reynolds number of 100,000. Results indicate that both lift and drag coefficients increase with the angle of attack. The highest lift coefficient was achieved using a plain flap at a deflection angle of 20° and an angle of attack of 10°, while the highest drag force occurred under the same conditions. Compared to the baseline (unmodified) airfoil, the lift-to-drag ratio improved significantly with flap deployment, reaching its maximum for a plain flap at a 10° deflection. The simulation outcomes were validated against available experimental data under comparable boundary conditions. These findings offer valuable guidance for optimizing airfoil-flap configurations, with direct implications for the design of more efficient wing and control surface systems in modern aircraft, ultimately contributing to enhanced fuel economy and overall aerodynamic performance.

Keywords: NACA 0015 Airfoil, Lift, Drag, Flap, Ansys, Static pressure.

1 Introduction

One of the first issues in the aviation industry has been the computation of lift and drag over different vehicle bodies. An airfoil is the cross-sectional state of a wing of a rotor, turbine, propeller, or sail which provides lift to the plane as well as drag [1]. The lift generation of a plane depends on the shape of the airfoil, wing area, and aircraft velocity [2]. An airplane's velocity is comparatively low during takeoff and landing. To maintain high lift to avoid objects on the ground airplane designers aim to increase wing area and modify airfoil shape by incorporating moving elements on the leading and trailing edges of the wings. The moving element on the leading edge is called a slat & the moving element on the trailing edge is called a flap. The addition of a flap and slat helps to control lift and drag according to the need of the airplane [3]. Previously, the calculation of lift & drag was performed through a trial-and-error method. But these days both analytical and computational methods are developed to closely approximate the lift coefficient and pressure distribution over a body. In this study, we will explore the effects of various types of flaps. The flap & slat of a running airfoil is shown in Fig. 1. Flow over an airfoil is shown in Fig. 2. Hasan et al. [4] conducted a comparison study by computing and testing the aerodynamic properties of the NACA 0012 and NACA 2412 airfoils. The turbulence models that were employed were $k-\omega$ SST Turbulence Model, Standard $k-\varepsilon$ Turbulence Model, Spalart-Allmaras Turbulence Model, $k-k_L-\omega$ Turbulence Model, and $\gamma-R_\theta$Transition SST Turbulence Model. At a lower angle of attack, these models were capable of determining the drag coefficients. However, none of those could precisely calculate the drag coefficient at a greater angle of attack.

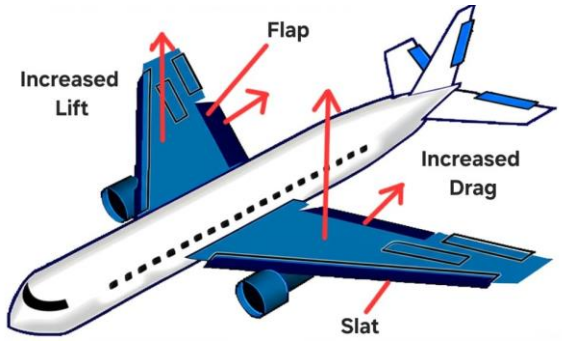

Fig. 1 Use of flap and slat on an airplane.

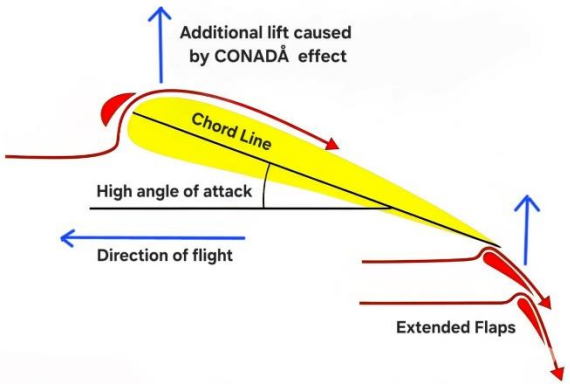

Fig. 2 Flow over an extended airfoil.

*Corresponding Author Email Address: atikkhan1603@outlook.com Published by: SciEn Publishing Group

The simulation results and the experimental results were compared [4]. Sharma and Poddar [5] experimented & found that NACA 0015 airfoil with a C = 0.31m and an AOA of -5° to 250° & Reynolds numbers ranging from 200000 to 600000 when the AOA increases, the laminar separation bubble bursts, the flow becomes turbulent, and the flow abruptly separates, causing "Abrupt Stall." [5]. Dionne and Lee [6] used NACA 0015 to determine the impact of trailing-edge flap deflection on the aerodynamic characteristics and flow field of a symmetric airfoil over a sinusoidal wave-like ground. The flap deflection causes a cyclic fluctuation in C_L and C_m across one wavelength, just as the unflapped airfoil. In contrast to C_L, the change in C_m shows a different pattern. However, compared to their unflapped counterparts, the flap deployment results in a bigger maximum and minimum C_L and C_m and a lesser fluctuation between these values. Comparing the flap-deflected airfoil to an unflapped airfoil at the wave valley results in higher RAM pressure and higher C_L [6]. Adem and Sahin [7] experimented to measure the lift & drag force of NACA 0015 airfoil. At different AOA & at low Reynolds numbers and found that drag and lift coefficients increased with increasing angle of attack. The stall was started with a 16° attack angle & the optimum lift coefficient value was measured and computed at 16° The optimum airfoil performance was measured and calculated at about 8° [7]. Rubel et al. [8] numerically & experimentally found that as the angle of attack is increased, the lift and drag coefficients for NACA 0015 airfoil both rises. As Reynolds' number rises, the drag coefficient steadily decreases. However, the lift coefficient increases slightly as Reynolds' number rises before beginning to decline [8]. Ahmed et al. [9] investigated a computational study on NACA 0012 airfoil having different flap angles at different Mach numbers & found that High flap angles result in a higher lift but it also increases drag very significantly. Furthermore, it is also obvious that decreasing flap angles causes an increase in range and endurance. Additionally, range and endurance for each flap angle decrease with rising Mach number [9]. Daud et al. [10] analyzed the effect of slat & flap on NACA 0015 airfoil where they found that when the slat angle is 25° & the flap angle is 30° then the lift coefficient became maximum.

2 Designed Model for CFD Analysis

3D & 2D view of NACA 0015 airfoil are shown in Fig. 3 and Fig. 4 respectively.

Fig. 3 3D view of NACA 0015

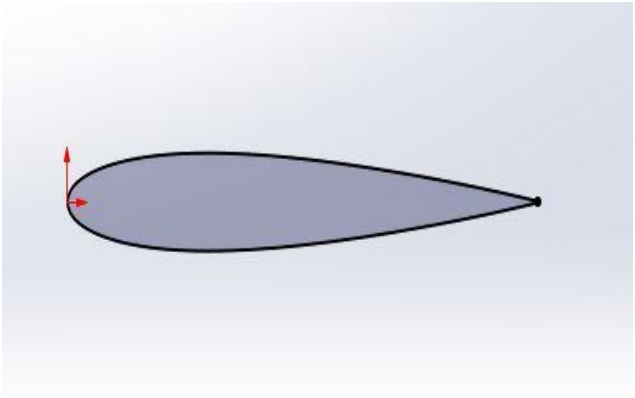

Fig. 4 2D view of NACA 0015

3D & 2D view of NACA 0015 airfoil with plain flap are shown in Fig. 5 and Fig. 6 respectively.

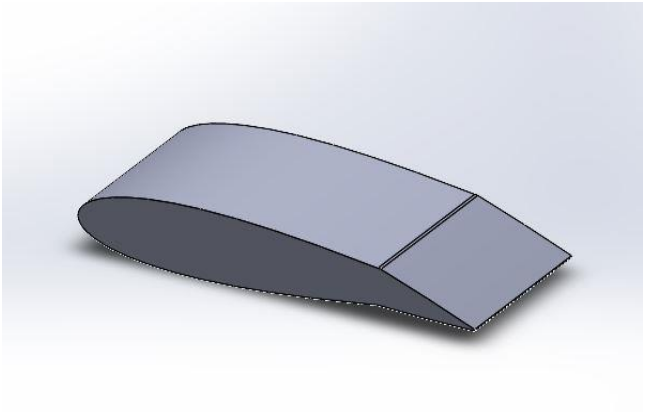

Fig. 5 3D view of NACA 0015 with plain flap

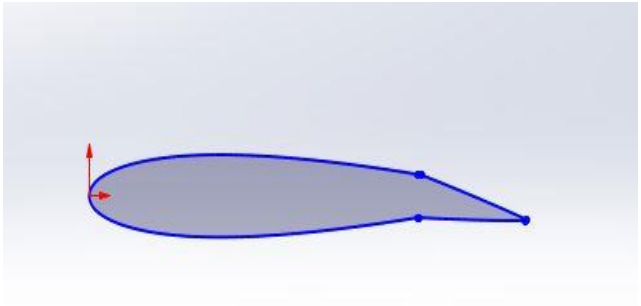

Fig. 6 2D view of NACA 0015 with plain flap

3D & 2D view of NACA 0015 airfoil with slotted flap are shown in Fig. 7 and Fig. 8 respectively.

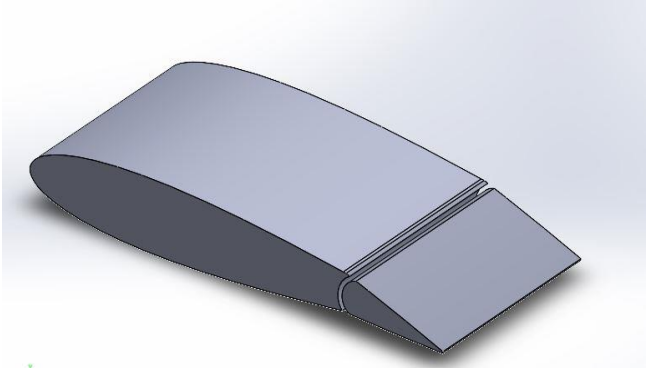

Fig. 7 3D view of NACA 0015 with slotted flap

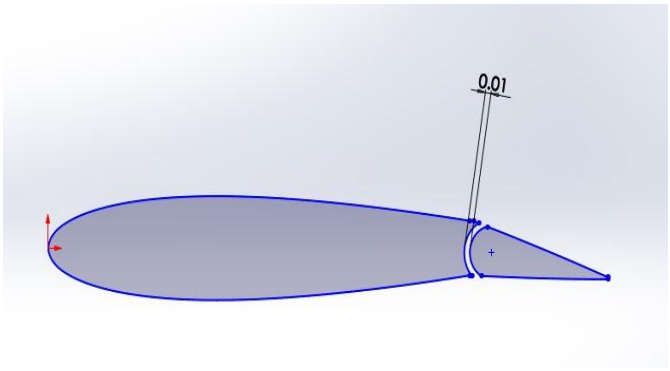

Fig. 8 2D view of NACA 0015 with slotted flap

In Table 1 specification of the used airfoil is given.

Table 1 Specifications of the used Airfoil.

NO	Description	Dimensions
1	Airfoil type	NACA 0015
2	Wing span	100 cm
3	Chord length	100 cm
4	Flap to chord ratio	25%C or 25 cm
5	Gap between flap and airfoil	1%C or 1 cm

Fig. 9 shows mesh generation of different types of airfoil profiles.

3 Governing Equation

In our study, we used the standard k–ω SST turbulence model to perform the simulations. This model is one of the most extensively used in engineering applications due to its balance of accuracy and robustness. Originally developed by Wilcox [11] as the standard k–ω model, it was later modified by Menter [12] to form the k–ω shear-stress transport (SST) model. The k–ω SST model is particularly well-suited for fully developed turbulent flows and offers improved prediction capabilities in both near-wall and free-stream regions. While the standard k–ε model performs well in the far field and the standard k–ω model is accurate near walls, the k–ω SST model blends the advantages of both through a hybrid formulation [13]. This makes it ideal for simulating flows with strong adverse pressure gradients and separation—conditions often encountered in airfoil aerodynamics. Therefore, the k–ω SST model was chosen over other turbulence models for its superior ability to capture the complex flow features around the airfoil and flap configurations accurately.

The $k-\omega$ SST turbulence model is governed by following equations:

$$\frac{D\rho k}{Dt} = \tau_{ij} \cdot \frac{\partial u_i}{\partial x_j} + \beta * \rho\omega k + \frac{\partial}{\partial x_j}\left[(\mu + \sigma_k \mu_t)\frac{\partial k}{\partial x}\right] \quad (1)$$

$$\frac{D\rho\omega}{Dt} = \frac{\gamma}{v_t}\tau_{ij}\frac{\partial u_i}{\partial x_j} - \beta\rho\omega^2 + \frac{\partial}{\partial x_j}\left[(\mu + \sigma_\omega \mu_t)\frac{\partial \omega}{\partial x_j}\right] + 2\rho(1-F_1)\sigma_\omega \frac{1}{\omega}\cdot\frac{\partial k}{\partial x_j}\cdot\frac{\partial \omega}{\partial x} \quad (2)$$

where, $\beta^* = \frac{\varepsilon}{K_\omega}$ and the turbulence stress tensor is,

$$\tau_{ij} = -\rho\overline{u_i' u_j'} = \mu_t\left(\frac{\partial u_i}{\partial x_j} + \frac{\partial u_j}{\partial x_i} - \frac{2}{3}\frac{\partial u_k}{\partial x_k}\delta_{ij}\right) - \frac{2}{3}\rho k\delta_{ij} \quad (3)$$

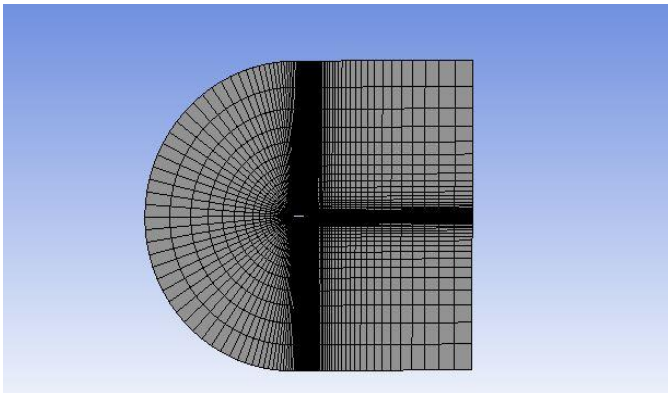

(a)

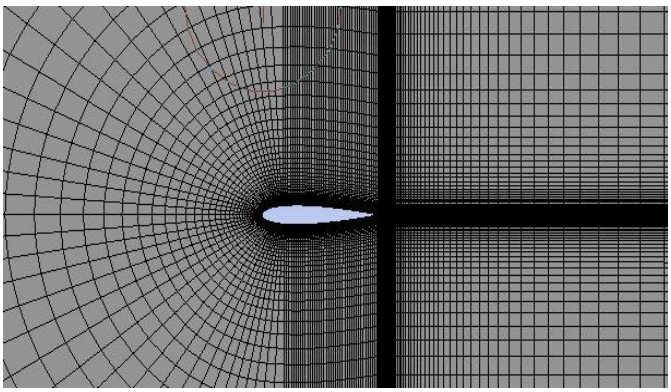

(b)

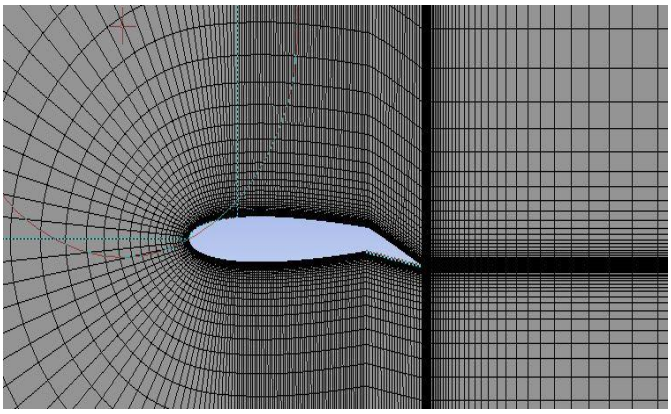

(c)

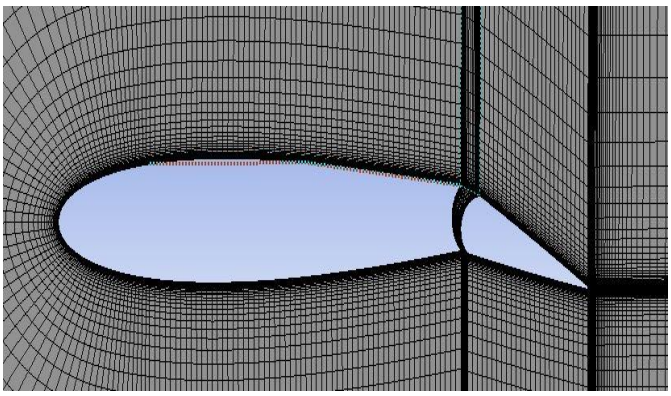

(d)

Fig. 9 Mesh of (a) whole flow domain of plain NACA 0015 (b) flow domain near airfoil NACA 0015 (c) flow domain near NACA 0015 airfoil with plain flap (d) flow domain near NACA 0015 airfoil with slotted flap

The turbulence viscosity can be determined by $v_t = a_1 \frac{k}{max[a_1,\omega,\Omega F_2]}$

where, Ω = the absolute value of the vorticity, a_1 =31.01 and the function F_2 is given by,

$$F_2 = tan\ h\left\{max\left[\left(\frac{2\sqrt{k}}{0.09\omega y}, \frac{500v}{y^2\omega}\right)\right]\right\}^2 \quad (4)$$

where, y is the distance to the nearest surface.

The coefficients $\beta, \gamma, \sigma_k, \sigma_\omega$ are defined as functions of the coefficients of the $k-\omega$ model which are defined as follows:

$$\beta = F_1\beta_1 + (1-F_1)\beta_2, \quad \gamma = F_1\gamma_1 + (1-F_1)\gamma_2, \quad (5)$$

$$\sigma_k = F_1\sigma_{k_1} + (1-F_1)\sigma_{k_2}, \qquad \sigma_\omega = F_1\sigma_{\omega_1} + (1-F_1)\sigma_{\omega_2} \quad (6)$$

where the function F_1 is,

$$F_1 = tanh\left\{min\left[max\left[\left(\frac{\sqrt{k}}{0.09\omega y}, \frac{500v}{y^2\omega}\right), \frac{4\rho\sigma\omega_2 k}{CD_{k\omega}y^2}\right]\right]\right\}^4 \quad (7)$$

and the coefficient $CD_{K\omega}$ is,

$$CD_{K\omega} = \max\left(2\rho\omega_2 \frac{1}{\omega}\frac{\partial k}{\partial x_j}\frac{\partial \omega}{\partial x_j}, 10^{-20}\right) \quad (8)$$

Model constants: β^*=0.09, β_1=0.075, β_2=0.0828, γ_1=0.5532, γ_2=0.4404, σ_{k_1} =0.85, σ_{k_2} =1.0, σ_{ω_1} =0.5 and σ_{ω_2} =0.856.

In this chapter, data obtained from numerical analysis is presented with the aid of tables. After that, validation of the numerical analysis is portrayed. However, significance of these data might be difficult to understand since no graphical method is used to characterize the aerodynamic properties by the obtained data in this chapter. In the validation part of this chapter, one graphical plot is shown in order to visualize the comparison between the data obtained from CFD analysis and practical experiment.

4 Data Obtained from Numerical Analysis

Table 2 shows the required data and boundary conditions for the simulation.

Table 2 Some essential data

Fluid type	Air
Airfoil material	Aluminum
Chord length of Airfoil	100 *cm*
Span	100 *cm*
Total area	$100 * 100\ cm^2$
Temperature	$20°C$
Gauge pressure	0 *Pa*
Velocity of air	$1.63\ m.s^{-1}$
Air density	$1.204\ kg.m^{-3}$
Viscosity of air	$1.82 \times 10^{-5} kg.m^{-1}.s^{-1}$
Reynolds number	$0.1 * 10^6$

4.1 Lift and Drag Coefficients for NACA 0015 Airfoil with Plain Flap

Lift and Drag coefficients obtained from simulation for NACA 0015 airfoil with plain flap are shown in Table 3, Table 4 and Table 5 respectively.

Table 3 Lift and Drag Coefficient of NACA 0015 airfoil with plain flap at flap angle 10°

AOA	Lift Coefficient (C_L)	Drag Coefficient (C_D)
0	0.370585	0.02456
5	0.803810	0.032945
10	1.162352	0.052314
12	1.186845	0.073808

Table 4 Lift and Drag Coefficient of NACA 0015 airfoil with plain flap at flap angle 15°

AOA	Lift Coefficient (C_L)	Drag Coefficient (C_D)
0	1.355312	0.091217
5	2.294319	0.114669
10	2.955348	0.171941
12	1.901588	0.507273

Table 5 Lift and Drag Coefficient of NACA 0015 airfoil with plain flap at flap angle 20°

AOA	Lift Coefficient (C_L)	Drag Coefficient (C_D)
0	0.506950	0.033691
5	0.951040	0.043394
10	1.290716	0.666760
12	0.425104	0.255108

4.2 Lift and Drag Coefficients for NACA 0015 Airfoil with Slotted Flap

Lift and Drag coefficients obtained from simulation for NACA 0015 airfoil with slotted flap are shown in Table 6, Table 7 and Table 8 respectively.

Table 6 Lift and Drag Coefficient of NACA 0015 airfoil with slotted flap at flap angle 10°

AOA	Lift Coefficient (C_L)	Drag Coefficient (C_D)
0	0.185871	0.030391
5	0.657451	0.038357
10	1.009587	0.059916
12	0.372013	0.184443

Table 7 Lift and Drag Coefficient of NACA 0015 airfoil with slotted flap at flap angle 15°

AOA	Lift Coefficient (C_L)	Drag Coefficient (C_D)
0	0.359956	0.03840
5	0.836546	0.047414
10	1.227739	0.06817
12	0.700783	0.33351

Table 8 Lift and Drag Coefficient of NACA 0015 airfoil with slotted flap at flap angle 20°

AOA	Lift Coefficient (C_L)	Drag Coefficient (C_D)
0	0.555761	0.046276
5	1.021809	0.056086
10	1.281246	0.087067
12	1.244119	0.327201

4.3 Lift and Drag Coefficient for Plain NACA 0015 Airfoil

Lift and Drag coefficients obtained from simulation for plain NACA 0015 airfoil is shown in Table 9.

Table 9 Lift and Drag Coefficient of NACA 0015 airfoil

AOA	Lift Coefficient (C_L)	Drag Coefficient (C_D)
0	0	0.0199
5	0.4648387	0.021618381
10	0.83526863	0.035667292
12	0.89174854	0.051354952

4.4 Lift-to-Drag Ratio

Lift-to-Drag ratio obtained from numerical analysis is shown in Table 10.

Table 10 Comparison of lift-to-drag ratio

AOA	Plain NACA 0015 Airfoil	NACA 0015 with plain flap			NACA 0015 with slotted flap		
		10°	15°	20°	10°	15°	20°
0	0	15.09	15.05	14.86	6.12	9.37	12.00
5	21.50	24.40	21.92	20.00	17.14	17.64	18.22
10	23.42	22.22	19.40	17.19	16.85	18.00	14.72
12	17.36	16.08	1.67	3.75	2.02	2.10	3.80

4.5 Data Validation

In Table 11 the comparison between experimental and numerical data has been shown. The experimental values have been collected from the experiment done by De Simone [14].

Table 11 Comparison of lift-to-drag ratio between experimental and numerical analysis

AOA	Numerical Data of NACA 0015	Experimental Data of NACA 0015
0	0	0
5	21.50	17.43
10	23.42	15.67
12	17.36	13

Fig. 10 exhibits validation of our CFD analysis using lift-to-drag ratio.

The data stated in this chapter have been used in the following chapter to generate different graphs and plots to comprehend the aerodynamic effect of using different types of flaps at different angle. Although the numerical results show a similar trend to the experimental data, some discrepancies are observed in the lift-to-drag ratio values. These differences primarily arise due to inherent limitations in the simulation model. Firstly, the CFD analysis was performed assuming a perfectly smooth airfoil surface, whereas in reality, the experimental model surface exhibits microscopic roughness. This surface roughness increases skin friction and affects boundary layer behavior, resulting in a lower lift-to-drag ratio in the experimental data.

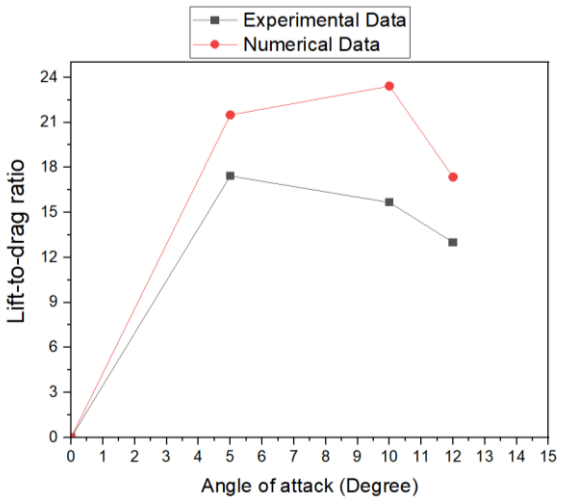

Fig. 10 Validation of CFD analysis using Lift-to-drag ratio

Secondly, the simulation considers an idealized geometry, free from any manufacturing imperfections or material inconsistencies. However, such imperfections are inevitable in physical experiments and can influence the aerodynamic performance. Moreover, the turbulence model used in the CFD setup—although robust—introduces certain limitations. It does not fully capture complex flow phenomena such as transitional flow, separation bubbles, or vortex shedding under varying flow conditions, particularly at higher angles of attack. The simulation was also conducted in two dimensions to reduce computational cost. This approach ignores three-dimensional flow effects such as tip vortices and spanwise pressure gradients that naturally occur in the experimental setup, contributing to the observed discrepancies. Finally, the boundary conditions in the simulation were set under ideal and uniform flow conditions, which are difficult to replicate precisely in wind tunnel experiments. Minor disturbances or measurement uncertainties in the experimental setup further contribute to the variation. Despite these differences, the overall agreement between the numerical and experimental results supports the validity of the CFD model for analyzing the aerodynamic characteristics of the airfoil under various configurations.

5 Comparative Analysis of The Results

In this part of the chapter, the graphical representations of lift coefficient, drag coefficient, lift to drag ratios and contours of static pressure have been discussed respectively. These data are plotted with respect to angles of attack, geometries having different at different angle.

5.1 Graphical Representation of Lift Coefficients

Comparison of Lift coefficients with respect to angle of attack is shown in Fig. 11. This graph is plotted using Table 3 to Table 9.

From the graph we can say that Lift coefficients increased with the increase of angle of attack and addition of flap also causes increase in lift coefficient.

5.2 Graphical Representation of Drag Coefficients

Comparison of Drag coefficients with respect to angle of attack is shown in Fig. 12. From the graph we can say that Drag coefficients increased with the increase of angle of attack and addition of flap also causes increase in drag coefficient and it is maximum for plain flap at 20^0 angle.

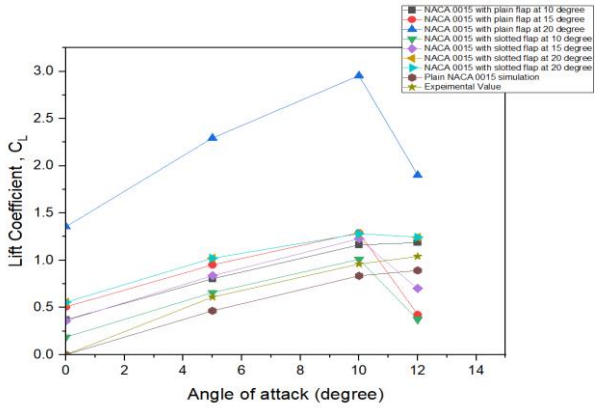

Fig. 11 Lift coefficient vs. angle of attack plot for different airfoil geometry.

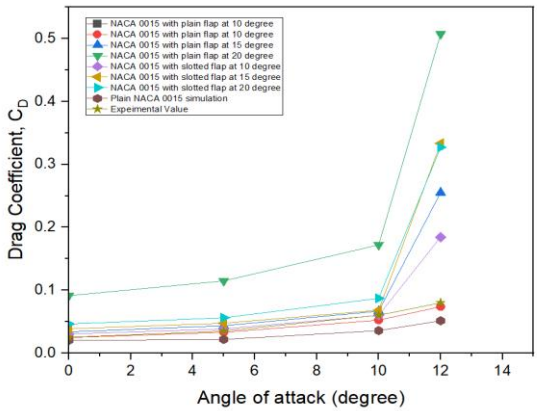

Fig. 12 Drag coefficient vs. angle of attack plot for different airfoil geometry.

5.3 Graphical Representation of Lift to Drag Ratios

Comparison of Drag coefficients with respect to angle of attack is shown in Fig. 13. From the graph we can say that Lift-to-drag coefficients increased with the increase of angle of attack and became maximum at 5^0 after that it stars decreasing and for plain flap it is maximum compared with slotted flap.

5.4 Contours of Static Pressure

The contours of static pressure generated by ANSYS are shown from Fig. 14 to Fig. 20. These figures project the distribution of static pressure around any airfoil geometry or any other geometry. These figures are formatted in such a way that the cooler tones indicate lower pressures where the warmer tones represent higher pressures.

5.4.1 Contours of Static Pressure of NACA 0015 Airfoil

Fig. 14 represents the contours of static pressure of plain NACA 0015 airfoil. The static pressure contours of the plain NACA 0015 airfoil demonstrate how pressure distribution changes with increasing angle of attack. At 0°, the flow is symmetric around the airfoil, resulting in negligible lift. As the angle increases to 5°, a clear pressure difference develops between the upper and lower surfaces, indicating the onset of lift generation. At 10°, this difference becomes more pronounced, enhancing lift further, although early signs of flow separation may start to appear. By 12°, the pressure field on the upper surface becomes more diffused, suggesting increased flow separation and the onset of stall. Overall, the contours clearly illustrate the relationship between angle of attack, pressure distribution, and lift performance.

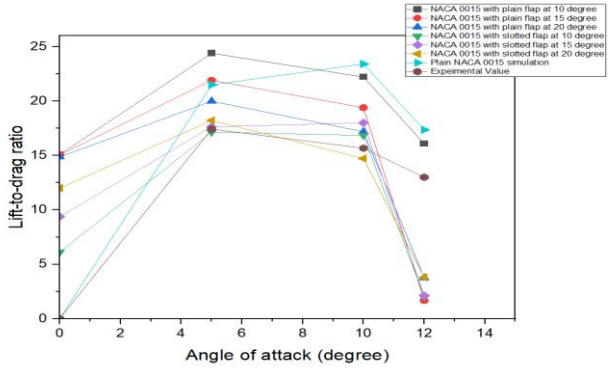

Fig. 13 Lift-to-drag ratio vs. angle of attack plot for different airfoil geometry

5.4.2 Contours of Static Pressure of NACA 0015 Airfoil with Plain Flap

Fig. 15 represents the contours of static pressure of NACA 0015 airfoil with plain flap at a flap angle of 10^0, 15^0 and 20^0. Fig. 15 presents the static pressure contours for the NACA 0015 airfoil equipped with a plain flap deflected at 10°, observed at various angles of attack (AOA). At 0°, the pressure distribution already shows asymmetry due to the flap deflection, resulting in noticeable lift even without geometric AOA. As the AOA increases to 5° and 10°, the low-pressure region on the upper surface expands, and the high-pressure zone on the lower surface intensifies, leading to enhanced lift generation. At 12°, flow separation becomes more evident near the trailing edge, as indicated by the weakening of the suction region and diffusion of the pressure gradient, marking the approach to stall conditions. The flap deflection enhances lift at lower AOAs but also accelerates the onset of separation at higher angles.

Fig. 16 illustrates the static pressure contours of the NACA 0015 airfoil with a 15° plain flap deflection at different angles of attack. Even at 0° AOA, the flap creates a significant pressure difference between the upper and lower surfaces, producing noticeable lift. As the AOA increases to 5° and 10°, the low-pressure zone on the suction side becomes stronger and more extended, while the pressure on the lower surface increases, resulting in greater lift. However, at 12°, the pressure contours on the upper surface begin to lose definition near the trailing edge, indicating early flow separation and reduced aerodynamic efficiency. This shows that while a 15° flap boosts lift at moderate AOAs, it also brings the flow closer to stall at higher angles.

Fig. 17 displays the static pressure contours for the NACA 0015 airfoil with a 20° plain flap deflection at various angles of attack. At 0° AOA, a strong pressure differential is already present due to the high flap angle, indicating substantial lift generation even without geometric inclination. As the AOA increases to 5° and 10°, the upper surface exhibits an expanded low-pressure region, while the lower surface shows elevated pressure, maximizing lift. However, at 12° AOA, the contours on the upper surface become less uniform and more scattered near the trailing edge, indicating significant flow separation. This confirms that while the 20° flap deflection yields the highest lift, it also causes a rapid decline in aerodynamic performance due to early stall onset.

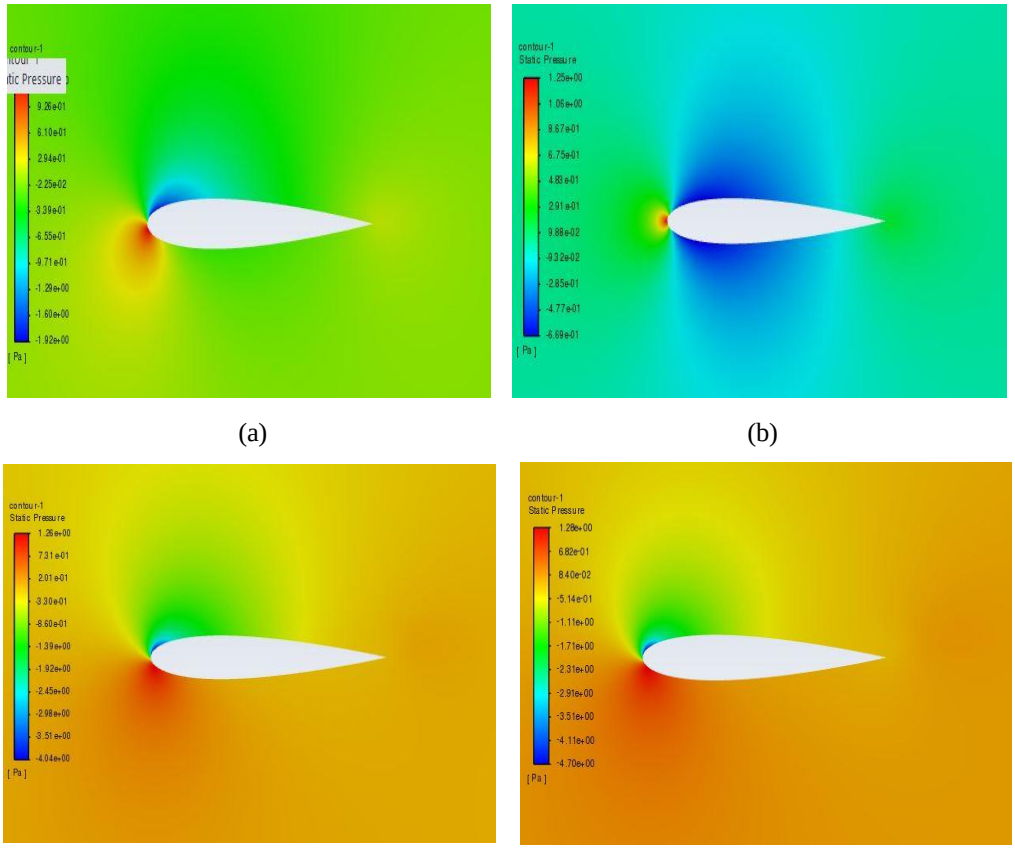

(a) (b)

(c) (d)

Fig. 14 Contours of static pressure of NACA 0015 airfoil at (a) AOA= 0°, (b) AOA= 5° , (c) AOA= 10° , (d) AOA= 12°

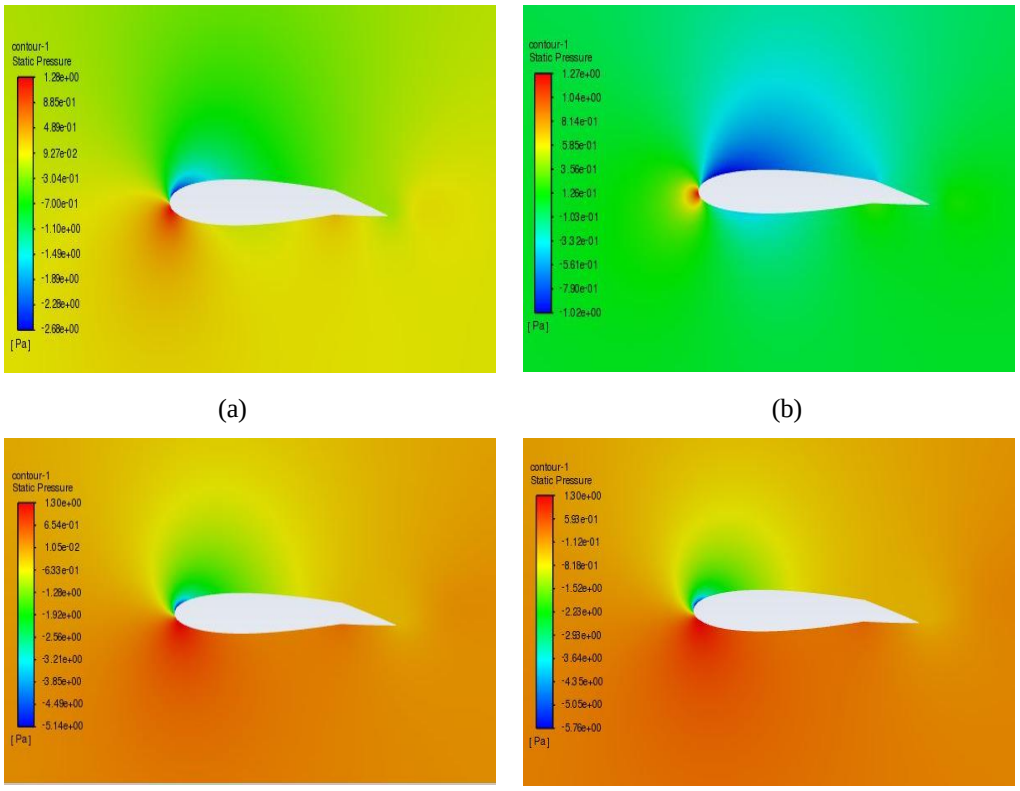

(a) (b)

(c) (d)

Fig. 15 Contours of static pressure of NACA 0015 airfoil with plain flap at 10°angle AOA= 0°, (b) AOA= 5° , (c) AOA= 10° , (d) AOA= 12°

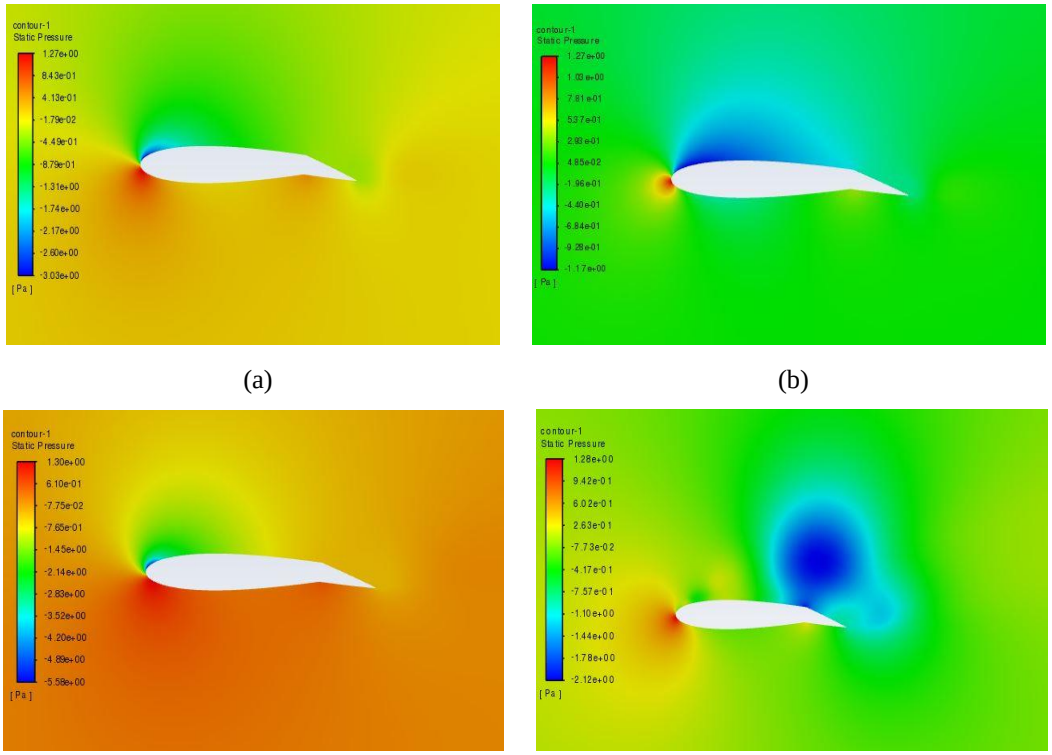

Fig. 16 Contours of static pressure of NACA 0015 airfoil with plain flap at 15°angle (a) AOA= 0°, (b) AOA= 5° , (c) AOA= 10° , (d) AOA= 12°

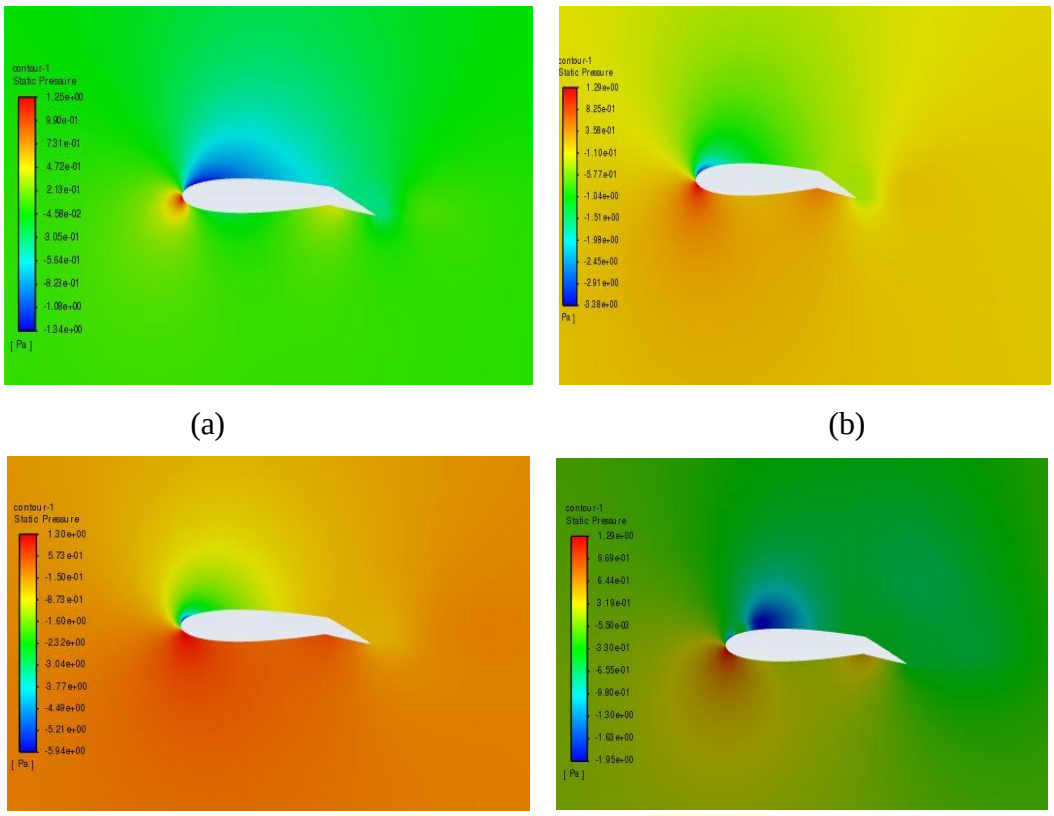

Fig. 17 Contours of static pressure of NACA 0015 airfoil with plain flap at 20°angle (a) AOA= 0°, (b) AOA= 5° , (c) AOA= 10° , (d) AOA= 12°

5.4.3 Contours of Static Pressure of NACA 0015 Airfoil with Slotted Flap

Fig. 18, Fig. 19, Fig. 20 respectively represents the contours of static pressure of NACA 0015 airfoil with slotted flap at a flap angle of 100, 150 and 200. Figure 18 shows the static pressure contours for the NACA 0015 airfoil equipped with a 10° slotted flap at different angles of attack. At 0° AOA, the flap creates a modest pressure difference, producing a small amount of lift. As the AOA increases to 5° and 10°, the suction on the upper surface strengthens, while the pressure on the lower surface increases, enhancing lift. The slotted design allows high-energy air to pass through the gap, delaying flow separation. At 12° AOA, the pressure contours remain relatively smooth and attached compared to plain flap configurations, indicating that the slotted flap effectively sustains flow attachment and resists stall onset at higher AOAs.

Fig. 19 presents the static pressure contours for the NACA 0015 airfoil fitted with a slotted flap deflected at 15° across varying angles of attack (AOA). At 0° AOA, the increased flap deflection generates a more pronounced pressure difference between the upper and lower surfaces compared to lower flap angles, resulting in higher baseline lift. As the AOA increases to 5° and 10°, the suction peak on the upper surface becomes stronger, while the pressure on the lower surface also increases significantly, indicating enhanced lift generation. The slotted flap effectively channels high-energy airflow through the slot, which helps maintain flow attachment over the airfoil and delays boundary layer separation. Even at 12° AOA, the pressure distribution remains relatively smooth and attached, suggesting that the 15° slotted flap configuration sustains aerodynamic performance and postpones stall onset better than smaller flap deflections or plain flap designs.

Fig. 20 displays the static pressure contours of the NACA 0015 airfoil with a slotted flap deflected at 20° for various angles of attack (AOA). At 0° AOA, the large flap deflection creates a significant pressure difference between the upper and lower surfaces, resulting in substantial lift generation even without angle of attack. As the AOA increases to 5° and 10°, the suction peak on the upper surface intensifies further, accompanied by a marked rise in pressure on the lower surface, indicating enhanced lift. However, the larger flap angle also increases the risk of flow separation. Despite the slotted flap's ability to energize the boundary layer by allowing airflow through the slot, at 12° AOA the pressure contours begin to show signs of flow detachment and potential stall onset. This suggests that while the 20° slotted flap provides high lift at lower AOAs, it also approaches its operational limits at higher angles, emphasizing a trade-off between lift enhancement and stall delay.

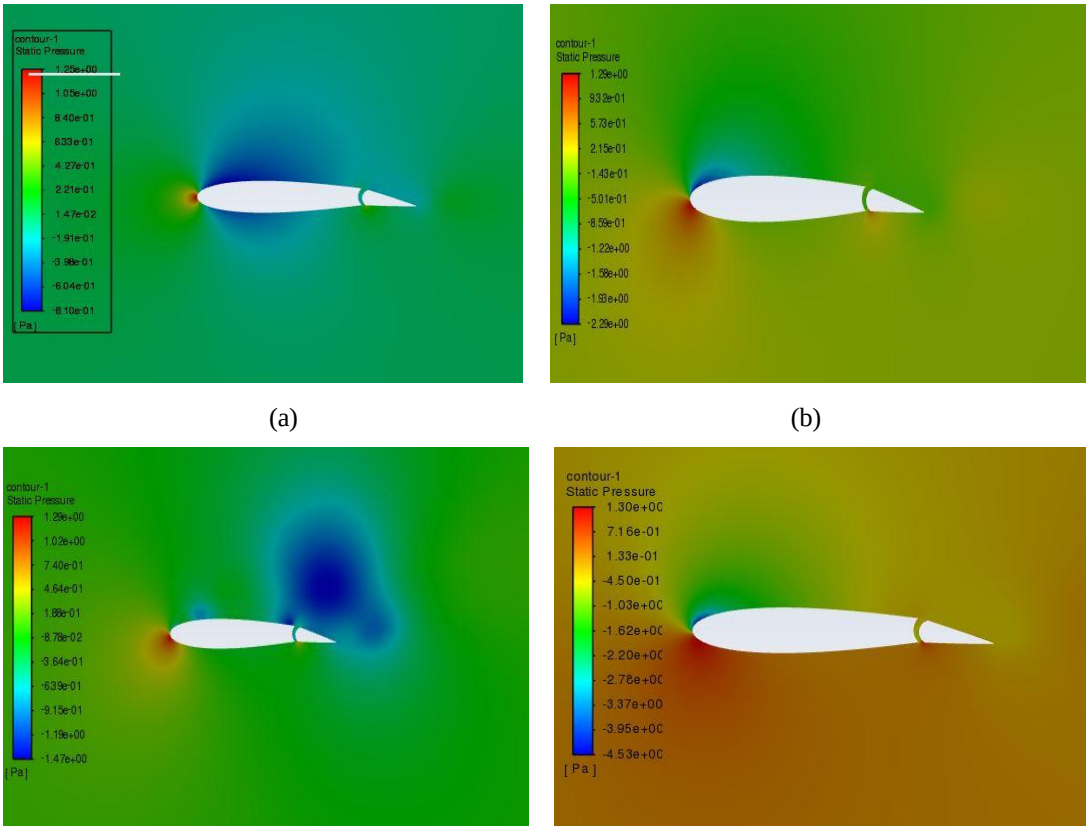

Fig. 18 Contours of static pressure of NACA 0015 airfoil with slotted flap at 10°angle AOA= 0°, (b) AOA= 5° , (c) AOA= 10° , (d) AOA= 12°

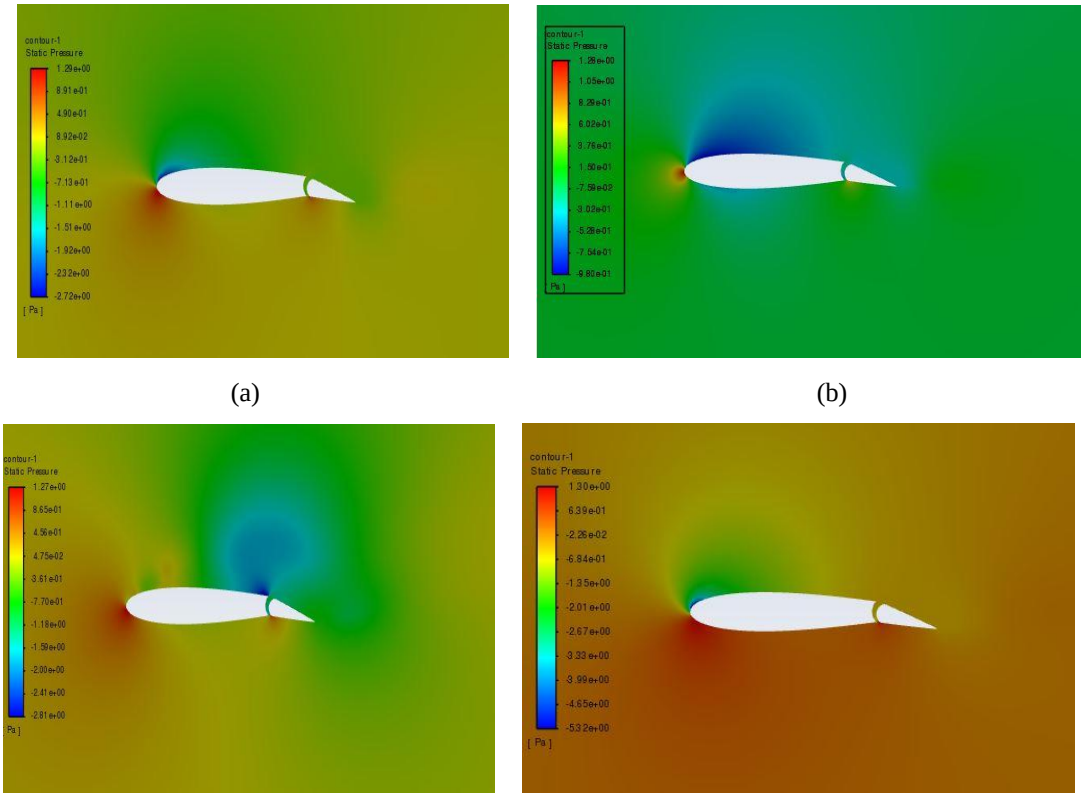

Fig. 19 Contours of static pressure of NACA 0015 airfoil with slotted flap at 15°angle (a) AOA= 0°, (b) AOA= 5° , (c) AOA= 10° , (d) AOA= 12°

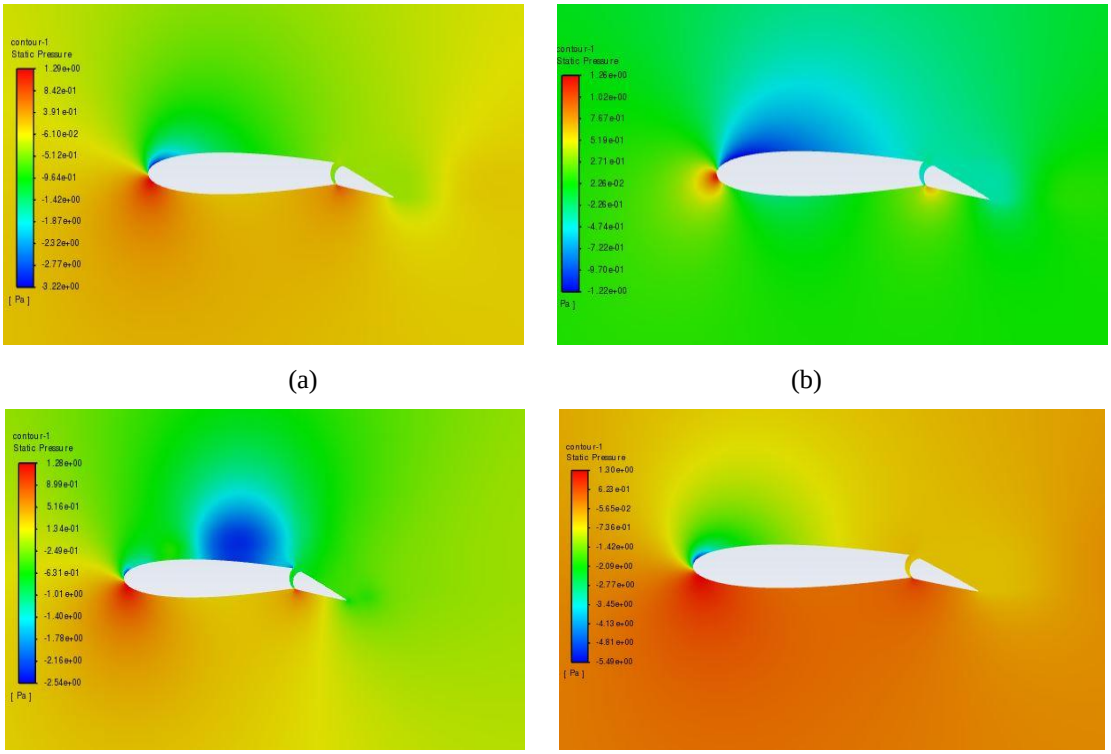

Fig. 20 Contours of static pressure of NACA 0015 airfoil with slotted flap at 20°angle (a) AOA= 0°, (b) AOA= 5° , (c) AOA= 10° , (d) AOA= 12°

To support both quantitative and qualitative analyses, numerical results were plotted alongside experimental data for comparison. Additionally, static pressure contours were generated to visualize the pressure distribution over the airfoil surface. These contours clearly show higher pressure on the lower surface and lower pressure on the upper surface in high-lift configurations, validating the aerodynamic mechanisms responsible for the observed trends.

6 Conclusion

The findings of this study can be concluded as follow:

- NACA 0015 airfoil produces zero lift at zero angle of attack whereas NACA 0015 airfoil with all flaps produces lift at zero angle of attack and it is the maximum for plain flap at flap angle 20^0.
- With the addition of flap lift coefficient increases in comparison with plain NACA 0015 airfoil. Lift coefficient maximizes for plain flap with 20^0 flap angle and for slotted flap the lift coefficient maximizes at 20^0 flap angles also.
- For plain NACA 0015 airfoil stall angle is found at 12^0 whereas with flap stall angle reduces and lies in between 10^0 to 11^0
- Drag coefficient increases with the increment of angle of attack and addition of flap also causes increase in drag coefficient but it increases drastically for plain flap at 20^0 angles.
- Lit-to-drag ratio for plain flap is greater than for slotted flap and lift-to-drag became maximum at an angle of attack 5^0 it starts decreasing after that.

Acknowledgements

The authors gratefully acknowledge the support and facilities provided by Chittagong University of Engineering and Technology, Chittagong, Bangladesh.

Author Contributions

Simanto Das: Conceptualization, Methodology, Software, Visualization; Md. Atikur Rahman Khan: Formal Analysis, Software, Writing – Original Draft; Sudipto Kumar Dash: Validation, Writing – Review & Editing, Visualization; Eyasin Hossain Sayeed: Resources, Formal Analysis, Methodology; Md. Mehdi Masud Talukder: Supervision

Conflict of Interest Statement

The authors declare that they have no known competing financial interests or personal relationships that could have appeared to influence the work reported in this paper.

Funding Information

This research did not receive any specific grant from funding agencies in the public, commercial, or not-for-profit sectors.

Generative AI Statement

Generative AI tools were not used in the writing, data analysis, or preparation of this manuscript. All content was developed solely by the authors.

References

[1] "Airfoil - Wikipedia." https://en.wikipedia.org/wiki/Airfoil (accessed Aug. 21, 2022).

[2] "Factors that Affect Lift." https://www.grc.nasa.gov/WWW/k-12/airplane/factors.html (accessed Aug. 21, 2022).

[3] "flap.gif (710×533)." https://www.grc.nasa.gov/www/k-12/airplane/Images/flap.gif (accessed Aug. 21, 2022).

[4] Hasan, S.M., Islam, S.M. and Haque, M., 2021. Comparison of aerodynamic characteristics of NACA 0012 and NACA 2412 airfoil. IJRASET, 9, pp.2037-2045.

[5] Sharma, D.M. and Poddar, K., 2010, October. Experimental investigations of laminar separation bubble for a flow past an airfoil. In Turbo Expo: Power for Land, Sea, and Air (Vol. 44014, pp. 1167-1173).

[6] Tremblay-Dionne, V. and Lee, T., 2019. Effect of trailing-edge flap deflection on a symmetric airfoil over a wavy ground. Journal of Fluids Engineering, 141(6), p.064501.

[7] Izzet ş., ACIR, A., 2015. Numerical and Experimental Investigations of Lift andDrag Performances of NACA 0015 Wind Turbine Airfoil. International Journal of Materials, Mechanics and Manufacturing,, 3(1).

[8] Rubel, R.I., Uddin, M.K., Islam, M.Z. and Rokunuzzaman, M.D., 2016. Numerical and experimental investigation of aerodynamics characteristics of NACA 0015 aerofoil. International Journal of Engineering Technologies IJET, 2(4), pp.132-141.

[9] Ahmed, T., Amin, M.T., Islam, S.R. and Ahmed, S., 2014. Computational study of flow around a NACA 0012 wing flapped at different flap angles with varying Mach numbers. Glob J Res Eng, 13(4), pp.4-16.

[10] Daud, N.M., Sudin, M.N. and Zakaria, M.S., 2022. Flow analysis of airfoil with mechanical slat and flap using CFD. *Journal of Engineering and Technology (JET)*, *13*(1), pp.73-82.

[11] Wilcox, D.C., 1988. Reassessment of the scale-determining equation for advanced turbulence models. AIAA journal, 26(11), pp.1299-1310.

[12] Menter, F.R., 1994. Two-equation eddy-viscosity turbulence models for engineering applications. AIAA journal, 32(8), pp.1598-1605.

[13] Aftab, S.M.A., Mohd Rafie, A.S., Razak, N.A. and Ahmad, K.A., 2016. Turbulence model selection for low Reynolds number flows. PloS one, 11(4), p.e0153755.

[14] De Simone, N., Cenedese, D., Aniello, A., De Simone, F. P. and De Simone, N., 2020. Wind Tunnel Testing of NACA 0015 and NACA 23012 Airfoils, Politecnico di Milano.